Heliyon 10 (2024) e25355

Contents lists available at ScienceDirect

Heliyon

journal homepage: www.cell.com/heliyon

Research article

Extraction of cellulose nanofibrils from pine sawdust by integrated chemical pretreatment

Xiaran Miao [a,b,c], Wenqiang Hua [c], Yiwen Li [c], Fenggang Bian [a,c,*], Tiqiao Xiao [a,c,**]

[a] Shanghai Institute of Applied Physics, Chinese Academy of Sciences, Shanghai, 201800, China
[b] University of Chinese Academy of Sciences, Beijing, 100049, China
[c] Shanghai Synchrotron Radiation Facility, Shanghai Advanced Research Institute, Chinese Academy of Sciences, Shanghai, 201204, China

ARTICLE INFO

Keywords:
Cellulose nanofibrils
Pine sawdust
Alkaline and acid-chlorite pretreatments
TEMPO-Oxidant
Integrated chemical pretreatment

ABSTRACT

Reducing energy consumption is major challenge in the industrialization of chemical pretreatments for the extraction of cellulose nanofibrils (CNF). In this study, an integrated chemical pretreatment with alkaline/acid-chlorite/TEMPO-oxidant was used for the nano-fibrillation of CNF from pine sawdust (WS). The alkaline and acid-chlorite pretreatments effectively eliminated the non-cellulosic components present in WS, resulting in the delamination of individual cell layers and swelling of the internal structures within the cellulose fiber bundles and cellulose microfibrils that form these layers. The spacing between CNF within the cellulose microfibrils increased from 3.7 nm to 5.5 nm. These loosely packed hierarchical structures facilitated the penetration of the reagent, which led to an increase in the specific surface area during the TEMPO-oxidant reaction and consequently accelerated the reaction rate. The WS was pretreated in a very dilute solution (1 % NaOH and 0.5 % $NaClO_2$) under mild conditions (70 °C for 1 h), which resulted in a significant reduction of the TEMPO reaction time (from 3 h to 30 min) and a lower consumption of the reaction reagent (one fourth of the amount consumed compared to the direct oxidation of WS to achieve the same degree of cellulose nano-fibrillation).

1. Introduction

As the most abundant biopolymer on Earth, cellulose nanofibrils (CNF) are attracting explosive interest as a renewable and low-carbon material due to theirs versatility and high performance [1]. CNF consist of linear polysaccharide chains with repeated β-1, 4-linked anhydro-glucose units (AGU), where each AGU has three hydroxyl groups that form strong hydrogen bonds. Because of these hydrogen bonds, the CNF are tightly bound together in the biomass, making them difficult to separate by simple treatments [2]. Despite the appealing properties and potential applications of CNF, the significant energy consumption required to produce them remains a barrier to widespread use [3]. Recent efforts have focused on reducing energy consumption to scale up CNF production from the laboratory to an industrial level. Lee et al. employed a dry grinding method, suggesting that a three-cycle shear cutting process was adequate for producing dry cellulose precursors for CNF production while reducing overall energy consumption [4]. Berto et al. used monocomponent endoglucanase for CNF extraction, achieving a nearly 100 % yield and reducing defibrillation energy by up to 50 % [5].

* Corresponding author. Shanghai Institute of Applied Physics, Chinese Academy of Sciences, Shanghai, 201800, China.
** Corresponding author. Shanghai Institute of Applied Physics, Chinese Academy of Sciences, Shanghai, 201800, China.
E-mail addresses: bianfg@sari.ac.cn (F. Bian), tqxiao@sari.ac.cn (T. Xiao).

https://doi.org/10.1016/j.heliyon.2024.e25355
Received 27 December 2023; Received in revised form 10 January 2024; Accepted 25 January 2024
Available online 29 January 2024
2405-8440/© 2024 The Authors. Published by Elsevier Ltd. This is an open access article under the CC BY-NC-ND license (http://creativecommons.org/licenses/by-nc-nd/4.0/).

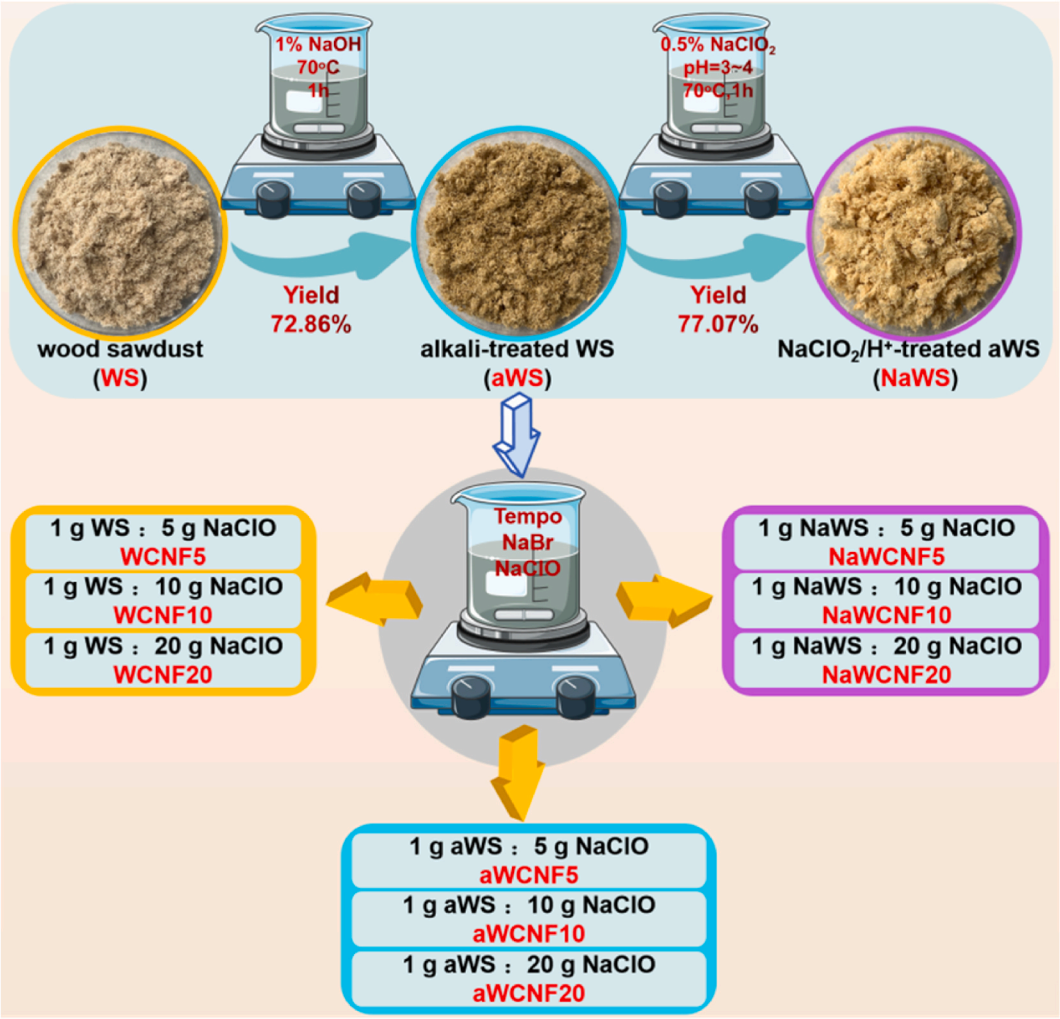

Fig. 1. Preparation process of CNF.

Pretreatment of cellulosic raw materials before nano-fibrillation can effectively reduce the cost of CNF production by removing non-cellulosic components, introducing functional groups, and swelling the fiber matrix. Over the years, numerous pretreatment methods have been explored [6], with chemical pretreatments being the most common. Chemical pretreatments are a highly versatile class of nano-fibrillation treatments for CNF. For instance, Peretz et al. using ozonation pretreatment followed by recyclable maleic acid hydrolysi for CNF production from recycled paper mill sludge [7]; Wang et al. isolated nanocellulose from hardwood pulp via phytic acid pretreatment [8]; Faria et al. produced CNF from pineapple crown fibers through alkaline pretreatment and acid hydrolysis under different conditions [9]. Chemical pretreatments introduce new charge groups on the cellulose surface that create repulsive forces that weaken hydrogen bonds cohesion [10]. Simplifying CNF separation and enabling the development of new functionalities [11].

Among chemical pretreatments, alkali treatments are the most commonly used methods, extensively applied in preparing raw materials for CNF production. Frequently, an alkaline treatment is combined with a bleaching step, typically utilizing sodium chlorite ($NaClO_2$), to enhance the removal of lignin residues. TEMPO oxidation is another significant strategy for CNF production due to its mild reaction conditions and the excellent quality of the CNF produced [12].

Wood residues, such as sawdust, are promising sources of cellulosic raw materials due to their abundance and low cost [13]. Woody commodities generally have a higher lignin content than agricultural commodities such as straw, hemp, or cotton. Pine wood, for example, contains about 28.4 % lignin [13], significantly higher than wheat straw (22.3 %), flax fiber (3.4 %) and cotton (1 %) [14,15]. Therefore, efficient removal of non-cellulosic components, especially lignin, is critical for effective extraction of CNF from pine sawdust. A detailed investigation is warranted to determine the pretreatment methods that can effectively reduce energy consumption when extracting CNF from pine sawdust.

In this study, an integrated chemical pretreatment method using alkali/acid-chlorite/TEMPO-oxidant is employed to extract CNF from pine sawdust. The morphology and chemical structure of both the pretreated wood sawdust and the produced CNF are

characterized in detail. At the same time, the study compares the time, reagent consumption, morphology, and chemical structure of the produced CNF between this integrated chemical pretreatment method and two other methods: alkali/TEMPO-oxidant pretreatment and single-step TEMPO-oxidant pretreatment. The results show that the alkali/acid-chlorite pretreatment can significantly reduces the consumption of chemical reagents and reaction time in the TEMPO oxidation process. For the extraction of CNF from woody materials, the alkali and acid-chlorite pretreatment processes in the mentioned integrated chemical pretreatment method are indispensable.

2. Materials and methods

2.1. Materials and reagents

Pine sawdust (WS, *Pinus Sylvestris Var. Mongholica Litv*) comes from a sawmill in Shanghai, China, and is sourced from Heilongjiang Province, China. The sawdust was crushed into powder with a length of several millimeters. To remove water-soluble impurities such as sediment, the sawdust was washed three times with deionized water and then dried in an oven at 50 °C for 24 h to remove moisture. The water used for the washing process was purified using a Milli-Q plus water purification system (Millipore Corporate, Billerica, MA). Analytically pure reagents such as sodium hydroxide (NaOH, 97 %), sodium chlorite ($NaClO_2$, 80 %), hydrochloric acid (HCl, 37 %), 2,2,6,6-tetramethylpiperidine-1-oxyl radical (TEMPO, 98 %), sodium bromide (NaBr, 99.6 %), and ethanol were purchased from Shanghai Aladdin Chemical Reagent Inc., China. Sodium hypochlorite (NaClO, 4.00–4.99 %) was purchased from Sigma-Aldrich. All reagents were used without further purification.

2.2. Extraction of CNF

Fig. 1 illustrates the manufacturing process of CNF. The washed WS was stirred in a 1 % NaOH solution at 70 °C for 1 h with a solid-liquid ratio of 1:50. The resulting WS was filtered, washed several times with deionized water, and dried in a 70 °C oven for 24 h. The resulting alkali-treated WS was designated as aWS. Subsequently, the dried aWS was immersed in a 0.5 % $NaClO_2$ solution with a solid-liquid ratio of 1:50. To prevent the introduction of impurities, hydrochloric acid (one drop of concentrated HCl per liter of solution) was used to adjust the pH of the solution to between 3 and 4. After stirring at 70 °C for 1 h, the acid-chlorite treated aWS was filtered, washed several times with deionized water, and dried for 24 h in a 70 °C oven. This dried product was named NaWS.

CNF were prepared using a previously described TEMPO/NaBr/NaClO oxidation system [12,16]. Specifically, 1.00 g NaWS was added to 50 mL deionized water, followed by NaBr (0.16 g) and TEMPO (0.016 g). This mixture was stirred for 0.5 h and then the reaction was initiated by adding different doses of NaClO solution (5.0 g/10.0 g/20.0 g). The pH was adjusted by adding 1 wt% NaOH solution to a value between 10.0 and 10.2 until the pH of the system did not change. The oxidation reaction was terminated by the addition of absolute ethanol (7.0 mL), followed by continuous stirring for 20 min. The oxidized pulps were then obtained and washed with deionized water, after a gentle mechanical homogenization resulting in CNF with a jelly-like consistency. The CNF thus prepared were named NaWCNF5/10/20. For comparison, CNF were also prepared from WS and aWS using the above steps and named WCNF5/10/20 and aWCNF5/10/20, respectively. 0.5 wt% CNF solutions were cast into a polytetrafluoroethylene (PTFE) mold, allowing for natural evaporation of water to obtain CNF films.

2.3. Characterization

The morphology of WS, aWS, NaWS, and CNF was visualized using a scanning electron microscope (SEM) (G3000, Zeiss, Germany) at an accelerating voltage of 4.6 kV and transmission electron microscopy (TEM) (TecnaiG2 F20 S-TWIN). The FTIR spectra of all samples were recorded using a Thermo Nicolet 6700 spectrometer (Thermo Fisher) from 4000 cm^{-1} to 500 cm^{-1} with a total of 64 scans. Thermal stability of the samples was analyzed using a thermal analyzer (2 SF/1100, Mettler Toledo, Switzerland) in the temperature range of 50–800 °C with a heating rate of 10 °C/min in a nitrogen environment.

Synchrotron radiation wide-angle X-ray scattering (WAXS)/small-angle X-ray scattering (SAXS) experiments were performed at BL16B1 beamline of Synchrotron Radiation Facility (SSRF, Shanghai, China). The wavelength used was 0.124 nm and the distance between the sample and detector was 97.8 mm and 1882.2 mm for WAXS and SAXS, respectively. Scattering patterns were recorded with a Pilatus 2 M detector and processed with Python-based software pyFAI (ESRF, Grenoble, France). Crystallinity index (*Cr*I) values were calculated using PeakFit (v4.12, SeaSolve Software Inc), which separates the background and overlapping peaks from the one-dimensional WAXS integral curves. The specific calculation method used is shown in Fig. S1 and follows a previously reported method [12]. The equatorial small-angle scattering intensity of WS, aWS, and NaWS was fitted with the function (2) based on the work of Paavo A. Penttilä [17].

$$I(q) = AI_{cry}(q, \overline{R}, \Delta R, a, \Delta a) + B\exp\left(\frac{-q^2}{2\sigma^2}\right) + Cq^{-\alpha} \tag{2}$$

where *A, B, σ, C* and *α* are constants, $I_{cyl}(q)$ is the intensity from the cylinder arrays. *R* represents the mean cylinder radius with standard deviation Δ*R*, while *α* represents the distance between the centers of the cylinders with paracrystalline distortion Δ*α* [18].

Optical photographs of CNF jelly and CNF films were taken with an iphone (iphone13 pro max). The micromorphology of CNF jelly was examined using a polarizing optical microscope (POM) (DM2500P, Leica, Germany). The surface charge of CNF in an aqueous

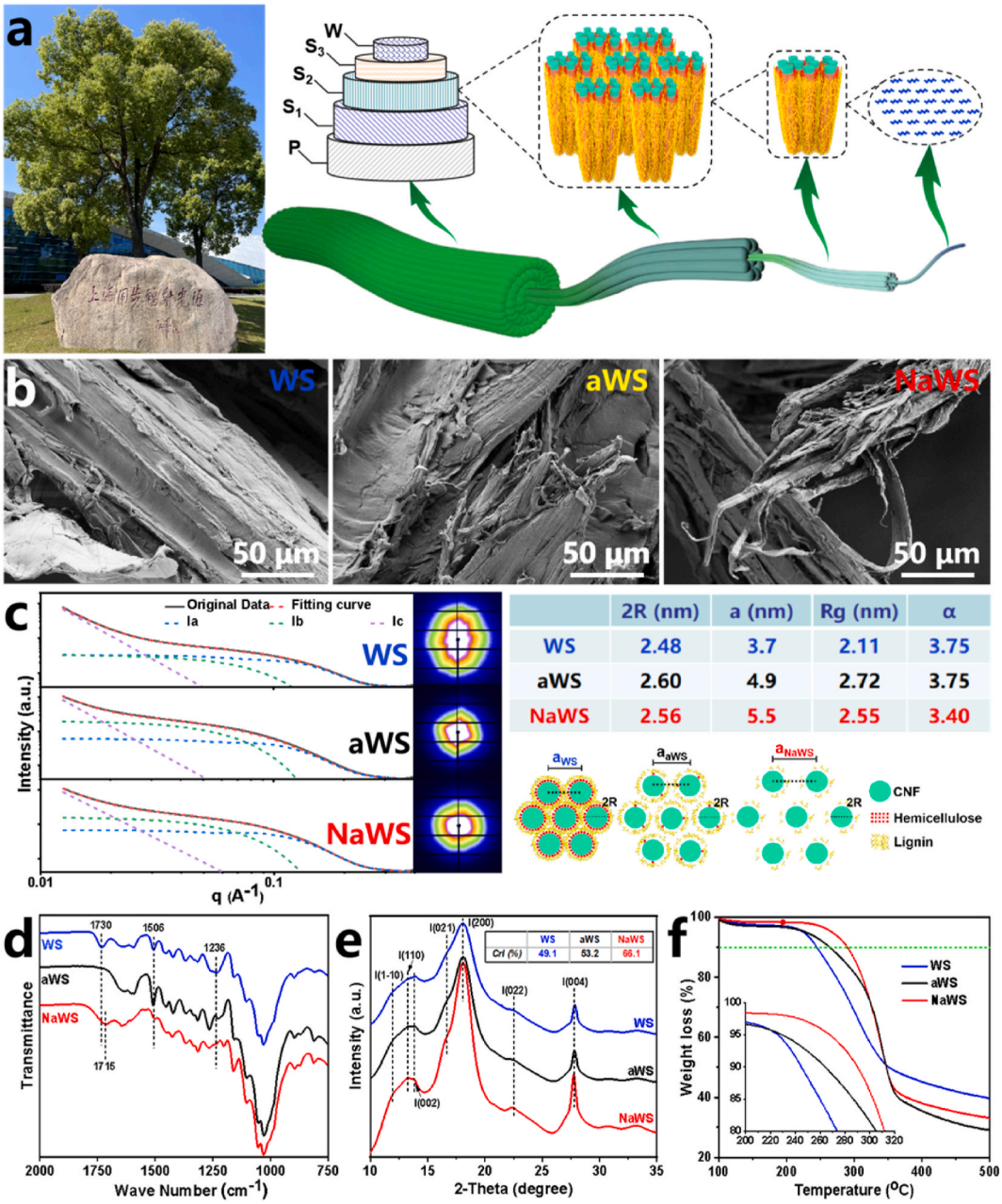

Fig. 2. (a)Hierarchical structures of wood biomass; (b)SEM images of WS, aWS and NaWS; (c)SAXS fitting results of WS, aWS and NaWS; (d)FTIR curves, (e)1D WAXS integral curves and (f)TGA curves of WS, aWS and NaWS.

suspension with the concentration of 0.01 wt% was measured using a Zetasizer Nano ZS (Malvern Instruments Ltd., Malvern, UK). The degree of carboxylation of TEMPO-oxidized CNF was determined by the titration method of electric conductivity [19].

3. Results and discussion

3.1. The structures and properties of pretreated pine sawdust

Fig. 2a illustrates the division of the cell walls of wood into three layers: the intercellular layer (M), primary wall (P), and the secondary walls (S1, S2, S3) [10]. These layers are distinguished based on the orientation, chemical composition, and stage of formation of the microfibers. The intercellular layer, located between two adjacent cell walls, is composed mainly of lignin and pectin substances and does not contain cellulose microfibers. Its main function is to bind and adhere to the cellulose microfibers. The primary

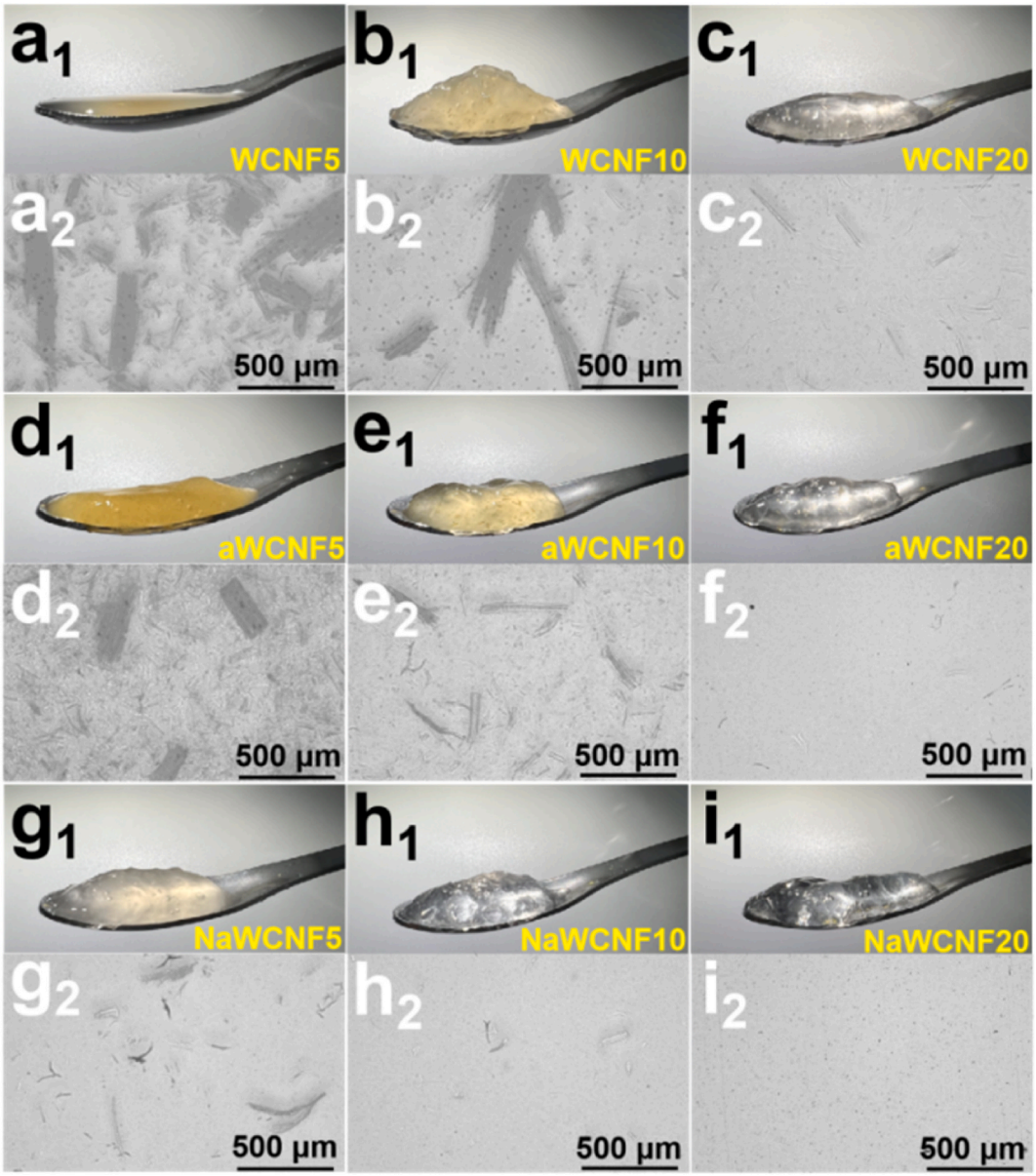

Fig. 3. The optical photographs (a_1-i_1) and the polarizing optical microscope photographs (a_2-i_2) of prepared CNF jelly extracted by the TEMPO oxidation.

wall, composed mainly of cellulose, hemicellulose, pectic substances, and a small amount of lignin, maintains and determines cell morphology and provides mechanical support. The secondary cell walls contain a large amount of lignin, which is highly cross-linked and reinforces the mechanical support required for upward growth. Each cell layer contains a hierarchical structure of cellulose fiber bundles, cellulose microfibrils that from the fiber bundles, and cellulose nanofibrils that from the cellulose microfibrils.

Chemical pretreatment of raw materials prior to TEMPO oxidation extraction of CNF aims to dissolve the intercellular layer, peel off to form individual cell wall layer, and efficiently remove non-cellulosic components wrapped around the surface of cellulose microfibers in the primary and secondary walls. This allows the chemical reaction reagents to directly reach the surface of the cellulose microfibers during the TEMPO oxidation process, improving the efficiency of the reaction. Fig. 2b shows SEM images which clearly illustrate how the single-laye cell wall (1–5 μm) in pine sawdust gradually detaches after alkaline (aWS) and acid-chlorite (NaWS) pretreatment.

Fig. 2c shows the SAXS fitting results of WS, aWS, and NaWS used to study the changes in the internal structure of cellulose microfibrils during alkaline and acid-chlorite pretreatments of pine sawdust. The "2R" listed in the table represents the average size of a single nanocellulose fiber and "a" represents the average distance between nanocellulose fibers. The fitting data show that the "2R"

values of WS, aWS, and NaWS remain almost unchanged (around 2.5 nm–2.6 nm), while the "a" value gradually increases. This indicates that after alkaline and acid-chlorite pretreatments, not only the single-layer cell wall was stripped, but also the interior of a single cellulose microfibril was relaxed and swollen due to the removal of hemicellulose and lignin. This resulted in an increase in the distance between the nanocellulose fibers in the cellulose microfibrils. In addition, the constant "2R" value (around 2.5 nm–2.6 nm) indicates that the alkaline and acid chlorite pretreatment do not affect the morphology of the individual nanocellulose fibers. Overall, the results of the SAXS and SEM images indicate that the hierarchical structures in the wood were loosened during the alkaline and acidic chlorite pretreatment of pine sawdust. This would be very beneficial for the subsequent process of nanocellulose fiber extraction by TEMPO oxidation.

The FTIR spectra of WS, aWS, and NaWS showed characteristic stretching vibration bands (2000-750 cm^{-1}) originating from the lignin, hemicellulose and cellulose components (see Fig. 2d). In the WS FTIR spectra, two strong absorption bands were observed at 1730 cm^{-1} (C═O stretching vibration of methyl ester) and 1236 cm^{-1} (C–O stretching vibration of acetyl in hemicellulose) [12], but almost disappeared in the aWS FTIR spectra, indicating the removal of hemicellulose during alkaline pretreatment. During the acid-chlorite pretreatment, a new reaction led to the formation of ether by the hydroxyl groups of cellulose in solution, resulting in cellulose with ester groups, as evidenced by the appearance of a new stretching vibration of ester groups at 1715 cm^{-1} in the NaWS FTIR spectra [20]. The WS and aWS FTIR spectra clearly showed the C═C stretching vibration of the aromatic skeleton in the lignin at 1506 cm^{-1} [12],which was less evident in the FTIR spectra of NaWS, suggesting that most of the lignin was removed in the acid-chlorite pretreatment but not in the alkaline pretreatment. Previous reports showed that pine sawdust contains 14.8 % hemicellulose, 28.4 % lignin, 4.7 % extractives, and 0.2 % ash [13]. The yield of alkaline pretreatment was 72.86 % (see Fig. 1), which removed almost all hemicellulose, extractives, ash, and a small amount of lignin from WS. The yield of acid-chlorite pretreatment was 77.07 % (see Fig. 1), which removed most of the remaining lignin.

The 1D integral curves obtained from the WAXS analysis data were used to examine the polymorphism of WS, aWS, and NaWS, as depicted in Fig. 2e. All three samples exhibited seven diffraction peaks at 11.8°, 13.2°, 13.9°, 16.6°, 18.1°, 22.2°, and 27.7°, corresponding to the characteristic (1-10), (110), (002), (021), (200), (022), and (004) lattice planes of cellulose I, respectively [12]. Thus, these data indicate that the cellulose polymorphism of pine sawdust did not change during alkaline and acid-chlorite pretreatments. As non-cellulosic substances such as hemicellulose and lignin were removed, the crystallinity of WS increased from 49.1 % to 53.2 % for aWS and 66.1 % for NaWS.

The thermal decomposition temperature of cellulose typically ranges between 200 °C and 315 °C. NaWS, predominantly composed of cellulose as depicted in Fig. 2f, exhibits a thermal decomposition temperature of approximately 230 °C, with a temperature for 5 % weight loss at around 270 °C. The decomposition temperature range of lignin is broader, spanning approximately 160 °C–900 °C, with the initial decomposition temperature lower than that of cellulose. Given that aWS contains a higher proportion of lignin compared to NaWS, the thermal decomposition temperature of aWS is lower than that of NaWS, and the decomposition rate is faster, as illustrated in Fig. 2f. The thermal decomposition temperature of aWS is approximately 200 °C, with a temperature for 5 % weight loss at around 235 °C. The thermal decomposition temperature of hemicellulose typically falls within the range of 150 °C–250 °C, comparable to the starting temperature of hemicellulose decomposition. WS contains a significant amount of hemicellulose, resulting in a thermal decomposition temperature similar to that of aWS (200 °C). The decomposition rate of WS is faster than that of aWS, with a temperature for 5 % weight loss at approximately 230 °C, and this difference in decomposition rates becomes more pronounced with increasing temperature.

3.2. The structures of prepared CNF

By adjusting the amount of oxidant (NaClO), CNF were extracted from WS, aWS, and NaWS using the TEMPO oxidation method. Optical photographs of the CNF aqueous solutions were shown in Fig. 3a_1-i_1 and Fig. S2 with a concentration of 0.5 wt%, and the micromorphology of CNF jelly observed by POM shown in Fig. 3a_2-i_2. Optical photographs showed that all CNF, except WCNF5, had a gel-like appearance. This may be attributed to the presence of numerous hydroxyl and carboxyl functional groups on the surface of CNF prepared by the TEMPO oxidation method. When the CNF concentration reached a certain level, the interactions such as electrostatic, hydrogen bonding and van der Waals forces between CNF were enhanced, resulting in stronger bonding and the formation of a three-dimensional network structure. This network structure was able to trap and fix a large amount of water molecules, forming a hydrogel. It is obvious that a certain amount of CNF was produced during these TEMPO oxidation processes, except for WCNF5.

When using WS for CNF extraction through TEMPO oxidation, the oxidant fibrillated a small amount of CNF from WS at an oxidant to WS ratio of 5:1. However, numerous micrometer-sized coarse fibers remained. The oxidant was primarily utilized in removing non-cellulosic substances in the cell wall and adherent cellulose microfibrils. With the increasing amount of oxidant, the CNF of WS (WCNF10) gradually fibrillated, and the gel exhibited a yellow color (see Fig. 3b_1), indicating the presence of lignin and indicative of incomplete fibrillation of CNF. With a further increase in the amount of oxidant, the gel of WCNF20 became lighter and eventually transparent, indicating a decrease in lignin content and the formation of more individualized CNF. This conclusion can also be verified from the POM photographs of WCNF5/10/20 (see Fig. 3a_2-c_2). At 100 × magnification, it is clear that a considerable amount of unoxidized WS was present in WCNF5. As the amount of oxidant increased, the amount of unoxidized WS in WCNF gradually decreased. Until the ratio of oxidant to WS reached 1:20, a small amount of unoxidized WS could still be found in WCNF20.

During the alkaline pretreatment, the hemicellulose and a part of the lignin were removed, which made the internal structure of the cellulose microfibrils looser and increased the spacing between CNF. This facilitated solvent penetration onto the surface of the CNF, leading to faster oxidation and subsequent fibrillation of the CNF. Thus, when the ratio of oxidant to aWS was 1:5, CNF (aWCNF5) could be fibrillated from aWS (see Fig. 3d_1). When the amount of oxidant reached a ratio of 1:20, the prepared aWCNF20 hydrogel was

Table 1
The reaction time of TEMPO oxidation.

Samples	The amount of NaClO (g)		
	5	10	20
WCNF	>6 h	~3 h	~3 h
aWCNF	~5 h	~2 h	~2 h
NaWCNF	~30 min	~35 min	~40 min

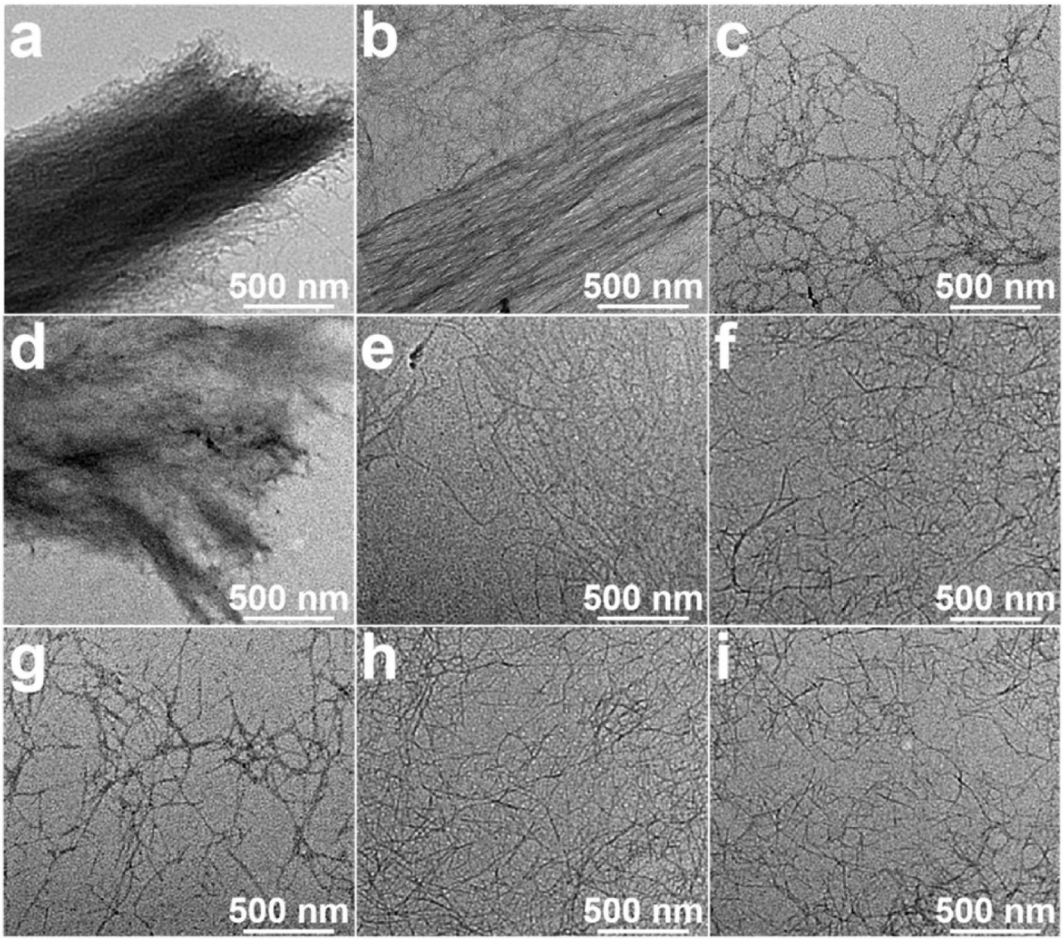

Fig. 4. TEM images of (a–c) WCNF5/10/15, (d–f) aWCNF5/10/15, (g–i) NaWCNF5/10/15.

completely transparent (see Fig. 3f_1), and no unoxidized aWS was observed (see Fig. 3f_2), indicating complete fibrillation of CNF from aWS. With further removal of lignin during the acid-chlorite pretreatment, the distance between CNF in NaWS further increased, which further improved the efficiency of CNF extraction from NaWS. The gel state of NaWCNF5 was almost similar to that of WCNF20 (see Fig. 3g_1), indicating that the consumption of oxidant by WS was four times higher than that of NaWS. Once the amount of oxidant reached a ratio of 1:10, all CNF could be completely fibrillated from NaWS (see Fig. 3h_2).

The removal of non-cellulosic materials gradually loosened the internal structures of NaWS, which facilitated the penetration of the reactant into the interior of the raw material fibers and the oxidation of the cellulose surface. This increased the specific surface area of the reaction and thus accelerated the reaction rate. As can be seen from Table 1, the reaction rate of NaWS was significantly higher than that of WS and aWS.

The TEM images shown in Fig. 4 provide a clear insight into the morphology of the CNF produced. It was difficult to discern the individual CNF in WCNF5 and aWCNF5, but the swollen cellulose microfibrils were discernible. In WCNF10, the mutually entangled CNF could be found, which gradually fibrillated from the cellulose microfibrils. With the increase of TEMPO oxidation degree, a considerable amount of intertwined CNF was observed despite the limited presence of cellulose microfibrils in NaWCNF5, aWCNF10, and WCNF20. The lengths of aWCNF10 and WCNF20 predominantly fall within the range of 400–800 nm, with NaWCNF5 being

Fig. 5. Transparency photographs of prepared CNF films.

slightly longer and primarily distributed between 500 and 900 nm (Fig. S3). Simultaneously, the diameter of CNF ranges from 5 to 40 nm, indicating incomplete nanofibrillation of CNF. These results were in agreement with the results shown in Fig. 3 for the optical microscopy images. As the degree of nano-fibrillation intensified, the aWCNF20 and NaWCNF10 exhibited a near absence of entangled CNF, predominantly showcasing individual CNF. Lengths were predominantly distributed between 100 and 600 nm (Fig. S3), with diameters around ~5 nm, approximating a individual CNF's diameter. This observation underscores the culmination of nano-fibrillation processes. Upon completion of CNF nano-fibrillation, residual oxidants in the reaction system would attack the amorphous regions of CNF, leading to their oxidation and dissolution. Removal of the amorphous domains caused the CNF to be broken, resulting in a decreased length. Consequently, NaWCNF20 exhibited shorter length (distributed between 0 and 400 nm) compared to aWCNF20 and NaWCNF10. Similar morphologies were evident in the microscopic images of SEM in Fig. S4.

The morphologies of the fabricated CNF could also be verified based on the transparency of the CNF films in Fig. 5. When the CNF contained a considerable amount of unreacted raw material, the CNF films were completely opaque. As the CNF were gradually delaminated, the transparency of the film increased until it became completely transparent. The transparency of the films from aWCNF20, NaWCNF10, and NaWCNF20 also confirmed the completion of CNF nano-fibrillation.

Fig. 6 illustrates the chemical and crystalline structures of the prepared CNF. In Fig. 6a–a prominent band at 1600 cm^{-1}, attributed to the stretching vibration of the sodium carboxylate group (COONa) [21], indicates the oxidation of hydroxyl groups to carboxyl groups on C6 of cellulose across all samples. The band at 1730 cm^{-1} in WCNF5, corresponding to the non-conjugated C═O stretching vibration in the hemicellulose carbonyl groups, gradually disappears in WCNF10 and WCNF20. This observation suggests that during CNF extraction from WS, a portion of the oxidant is consumed in the removal of hemicellulose. A similar trend is observed with the band at 1506 cm^{-1}, associated with the C═C stretching vibration of aromatic bonds in lignin. This band gradually disappeared in

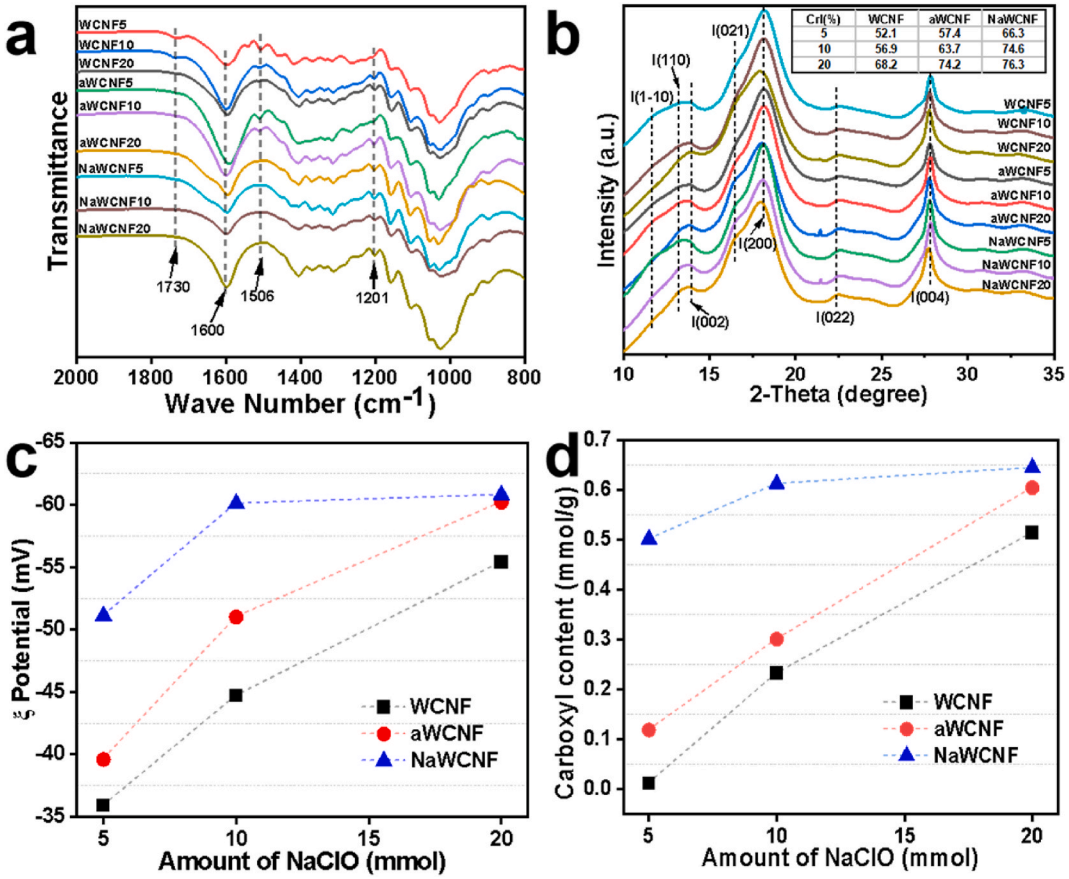

Fig. 6. (a) FTIR curves, (b) 1D WAXS integral curves, (c) Zeta potentials and (d) Carboxyl contents of prepared CNF.

WCNF10/20 and aWCNF10/20, confirming that in the preparation of CNF from both WS and aWS, part of the oxidant is utilized in lignin removal, thereby reducing the efficiency of nano-fibrillation. Notably, a new band at 1201 cm^{-1} emerged, suggesting the possibility that during the oxidation process, additional hydroxyl groups are oxidized to aldehyde or ketone groups. Similar situations are also evident in the raw material after acid-chlorite pretreatment, as depicted in Fig. 2d.

The TEMPO oxidation process did not alter the crystalline structure of CNF, as confirmed by the presence of seven characteristic lattice planes ((1-10), (110), (002), (021), (200), (022), and (004)) of cellulose I in the 1D integrated WAXS curves of all CNF (see Fig. 6b). As the degree of nano-fibrillation increases, the crystallinity of the prepared CNF also increases (see the insert in Fig. 6b). The crystallinity of NaWCNF20 was higher than that of aWCNF20 and NaWCNF10, confirming the dissolution of the amorphous regions and the rupture of the CNF in NaWCNF20.

The chemical structures of the prepared CNF were also studied by determining their zeta potentials and carboxyl contents. The zeta potentials are a measure of the density of carboxyl functional groups on the cellulose surface. From Fig. 6c and d, it can be seen that the trends in zeta potentials and carboxyl contents are similar. It is obvious that with an increase in oxidant dosage, the number of hydroxyl groups oxidized to carboxyl groups on C6 of CNF also increased. At relatively low oxidant dosages, the carboxyl content in NaWCNF was significantly higher compared to aWCNF and WCNF. This observation supports the idea that the removal of non-cellulosic components, such as hemicellulose and lignin from NaWS, along with the delamination of cellulose layers and the loosening of the internal structure of cellulose bundles, strongly promotes the oxidation of hydroxyl groups at C6 in CNF, facilitating nano-fibrillation. The quantity of carboxyl groups generated during the oxidation of NaWS with an oxidant ratio of 1:5 was nearly equivalent to that produced during the oxidation of WS with an oxidant ratio of 1:20. As the oxidant dosage increases, the individualization of NaWCNF has already been accomplished, and the excess oxidant is utilized in dissolving the amorphous regions of CNF. Consequently, the carboxylate content in NaWCNF20 did not exhibit a significant increase.

4. Conclusion

Through alkaline and acid-chlorite pretreatments, the cell walls of pine wood sawdust were not only cleaved into single-layer but also induced the loosening and expansion of cellulose fiber bundles and cellulose microfibrils constituting these cell layers. The distance between cellulose microfibrils within the cellulose microfibrils increases from 3.7 nm to 5.5 nm. During the TEMPO oxidation

process, the loosening of these multilayer structures and the increased distance between cellulose fibers facilitate the penetration of reactants into the interior, enabling the direct oxidation of cellulose surfaces and enhancing the efficiency of cellulose nanofibrillation. In comparison to the direct oxidation of WS for preparing CNF, NaWS undergone pretreatment only in extremely dilute solutions (1 % NaOH and 0.5 % $NaClO_2$) under mild conditions (70 °C, 1 h). This significantly reduced the TEMPO reaction time (from 3 h to 30 min) and decreased the amount of reaction reagents required (one-fourth of the WS amount required for the same degree of cellulose nanofibrillation). Despite the addition of two pretreatments, the reagents used in alkaline pretreatment can be reused, and the amount of reagents used in acid chlorite pretreatment is much less than the reduction in reagent usage during TEMPO oxidation. Moreover, the total time for the three reaction steps is less than the time required for direct oxidation from WS. Hence, the pretreatment steps involving the removal of hemicellulose and, notably, lignin, are essential for the extraction of CNF from woody raw materials.

Data availability statement

All relevant data are within the manuscript and its supplementary material.

CRediT authorship contribution statement

Xiaran Miao: Writing – review & editing, Writing – original draft, Data curation. **Wenqiang Hua:** Methodology. **Yiwen Li:** Methodology. **Fenggang Bian:** Methodology, Investigation. **Tiqiao Xiao:** Methodology, Investigation.

Declaration of competing interest

The authors declare the following financial interests/personal relationships which may be considered as potential competing interests:We declare that we have no financial and personal relationships with other people or organizations that can inappropriately influence our work, there is no professional or other personal interest of any nature or kind in any product, service and/or company that could be construed as influencing the position presented in, or the review of, the manuscript entitled. If there are other authors, they declare that they have no known competing financial interests or personal relationships that could have appeared to influence the work reported in this paper.

Acknowledgements

This work was supported by the *Youth Innovation Promotion Association of the Chinese Academy of Sciences* (No.2022288), the *National Nature Science Foundation of China* (No.12005285) and the Science and Technology Innovation Programme of Shanghai (grant No.22DZ2203000).

Appendix A. Supplementary data

Supplementary data to this article can be found online at https://doi.org/10.1016/j.heliyon.2024.e25355.

References

[1] K. Li, D. McGrady, X. Zhao, D. Ker, H. Tekinalp, X. He, J. Qu, T. Aytug, E. Cakmak, J. Phipps, S. Ireland, V. Kunc, S. Ozcan, Surface-modified and oven-dried microfibrillated cellulose reinforced biocomposites: cellulose network enabled high performance, Carbohydr. Polym. 256 (2021) 117525.
[2] F. Rol, M.N. Belgacem, A. Gandini, J. Bras, Recent advances in surface-modified cellulose nanofibrils, Prog. Polym. Sci. 88 (2019) 241–264.
[3] S. Sinquefield, P.N. Ciesielski, K. Li, D.J. Gardner, S. Ozcan, Nanocellulose Dewatering and drying: Current state and future perspectives, ACS Sustain. Chem. Eng. 8 (2020) 9601–9615.
[4] H. Lee, S. Mani, Mechanical pretreatment of cellulose pulp to produce cellulose nanofibrils using a dry grinding method, Ind. Crop. Prod. 104 (2017) 179–187.
[5] G.L. Berto, B.D. Mattos, O.J. Rojas, V. Arantes, Single-step fiber pretreatment with monocomponent endoglucanase: defibrillation energy and cellulose nanofibril quality, ACS Sustain. Chem. Eng. 9 (2021) 2260–2270.
[6] K. Copenhaver, K. Li, L. Wang, M. Lamm, X. Zhao, M. Korey, D. Neivandt, B. Dixon, S. Sultana, P. Kelly, W.M. Gramlich, H. Tekinalp, D.J. Gardner, S. MacKay, K. Nawaz, S. Ozcan, Pretreatment of lignocellulosic feedstocks for cellulose nanofibril production, Cellulose 29 (2022) 4835–4876.
[7] R. Peretz, E. Sterenzon, Y. Gerchman, V. Kumar Vadivel, T. Luxbacher, H. Mamane, Nanocellulose production from recycled paper mill sludge using ozonation pretreatment followed by recyclable maleic acid hydrolysis, Carbohydrate Polymers 216 (2019) 343–351.
[8] L. Wang, X. Zhu, X. Chen, Y. Zhang, H. Yang, Q. Li, J. Jiang, Isolation and characteristics of nanocellulose from hardwood pulp via phytic acid pretreatment, Ind. Crop. Prod. 182 (2022).
[9] L.U.S. Faria, B.J.S. Pacheco, G.C. Oliveira, J.L. Silva, Production of cellulose nanocrystals from pineapple crown fibers through alkaline pretreatment and acid hydrolysis under different conditions, J. Mater. Res. Technol. 9 (2020) 12346–12353.
[10] T. Yi, H. Zhao, Q. Mo, D. Pan, Y. Liu, L. Huang, H. Xu, B. Hu, H. Song, From cellulose to cellulose nanofibrils-A comprehensive review of the preparation and modification of cellulose nanofibrils, Materials 13 (2020).
[11] O. Nechyporchuk, M.N. Belgacem, J. Bras, Production of cellulose nanofibrils: a review of recent advances, Ind. Crop. Prod. 93 (2016) 2–25.
[12] L. Song, X. Miao, X. Li, F. Bian, J. Lin, Y. Huang, A tunable alkaline/oxidative process for cellulose nanofibrils exhibiting different morphological, crystalline properties, Carbohydr. Polym. 259 (2021) 117755.
[13] A. Ämmälä, O. Laitinen, J.A. Sirviö, H. Liimatainen, Key role of mild sulfonation of pine sawdust in the production of lignin containing microfibrillated cellulose by ultrafine wet grinding, Ind. Crop. Prod. 140 (2019).

[14] V. Menon, M. Rao, Trends in bioconversion of lignocellulose: biofuels, platform chemicals & biorefinery concept, Prog. Energy Combust. Sci. 38 (2012) 522–550.
[15] S.V. Vassilev, D. Baxter, L.K. Andersen, C.G. Vassileva, T.J. Morgan, An overview of the organic and inorganic phase composition of biomass, Fuel 94 (2012) 1–33.
[16] T. Saito, A. Isogai, Introduction of aldehyde groups on surfaces of native cellulose fibers by TEMPO-mediated oxidation, Colloids Surf. A Physicochem. Eng. Asp. 289 (2006) 219–225.
[17] P.A. Penttila, L. Rautkari, M. Osterberg, R. Schweins, Small-angle scattering model for efficient characterization of wood nanostructure and moisture behaviour, J. Appl. Crystallogr. 52 (2019) 369–377.
[18] H. Horiyama, K. Kojiro, Y. Okahisa, T. Imai, T. Itoh, Y. Furuta, Combined analysis of microstructures within an annual ring of Douglas fir (Pseudotsuga menziesii) by dynamic mechanical analysis and small angle X-ray scattering, J. Wood Sci. 68 (2022).
[19] B. Seantier, D. Bendahou, A. Bendahou, Y. Grohens, H. Kaddami, Multi-scale cellulose based new bio-aerogel composites with thermal super-insulating and tunable mechanical properties, Carbohydr. Polym. 138 (2016) 335–348.
[20] V.d.C. Correia, V. dos Santos, M. Sain, S.F. Santos, A.L. Leão, H. Savastano Junior, Grinding process for the production of nanofibrillated cellulose based on unbleached and bleached bamboo organosolv pulp, Cellulose 23 (2016) 2971–2987.
[21] A. Zitting, A. Paajanen, P.A. Penttilä, Impact of hemicelluloses and crystal size on X-ray scattering from atomistic models of cellulose microfibrils, Cellulose 30 (2023) 8107–8126.